

UC Irvine

UC Irvine Previously Published Works

Title

Demonstration of 3-band spatial frequency domain imaging using an 8-tap CMOS image sensor resistant to subject motion and ambient light

Permalink

<https://escholarship.org/uc/item/41p411sw>

ISBN

978-1-5106-4773-2

Authors

Takada, Kazuki
Shimada, Yuto
Yasutomi, Keita
[et al.](#)

Publication Date

2022-03-02

DOI

10.1117/12.2608412

Copyright Information

This work is made available under the terms of a Creative Commons Attribution License, available at <https://creativecommons.org/licenses/by/4.0/>

Peer reviewed

Demonstration of 3-band spatial frequency domain imaging using an 8-tap CMOS image sensor resistant to subject motion and ambient light

Kazuki Takada^{*a}, Yuto Shimada^{*a}, Keita Yasutomi^{*b}, Shoji Kawahito^{*b}, Gordon T Kennedy^{*c},
Anthony J Durkin^{*c, d}, and Keiichiro Kagawa^{*b}

^aGraduate School of Integrated Science and Technology, Shizuoka University

^bResearch Institution of Electronics, Shizuoka University

^cBeckman Laser Institute, University of California, Irvine

^dBiomedical Engineering Department, University of California, Irvine

ABSTRACT

We have developed a motion-resistant three-wavelength spatial frequency domain imaging (SFDI) system using an 8-tap CMOS image sensor. We have successfully measured two wavelengths using the same sensor. However, to remove the effect of melanin, measuring at three wavelengths is needed. In this study, the Hilbert transform is introduced to reduce the number of captured images for each wavelength from three to two. In the experiments, a DMD was illuminated with LEDs with wavelengths of 660nm, 780nm, and 850nm. One plane and one sinusoidal pattern were projected on the specimen for each wavelength. In addition, one ambient light image was captured to extract only the reflection components for the projected patterns. Pattern projection and exposure were repeated multiple times at a faster frame rate than the video rates to suppress the motion artifact while keeping appropriate signal levels. Totally 7 images were captured at once. Using this system, we demonstrated suppression of motion artifacts and ambient light in capturing a moving wrist.

Keywords: Spatial frequency domain imaging, quantitative tissue imaging, Hilbert transform, multi-band imaging, multi-tap CMOS image sensor

1. INTRODUCTION

We have developed a motion-resistant three-wavelength spatial frequency domain imaging (SFDI) system using a laboratory-designed 8-tap CMOS image sensor[1]. We have successfully measured the oxy-/deoxy-hemoglobin concentrations, total hemoglobin, and tissue oxygen saturation by simultaneously measuring the absorption and reduced scattering coefficients at two wavelengths with this sensor. However, to remove the effect of melanin absorption, measurement at least three wavelengths is crucial. We introduce the Hilbert transform[2, 3], which allows us to reduce the number of projection patterns for each wavelength from three to two. In this study, we use three light sources of 660nm, 780nm, and 850nm to separate the absorption of oxy-/deoxy-hemoglobin and melanin. Two images, plane and sinusoidal images, are taken at each wavelength to measure the reflectance at two different spatial frequencies. Then, absorption and reduced scattering coefficients are estimated by referring a look-up table for an assumed tissue model. In order to eliminate the bias caused by ambient light, which is one of the drawbacks of active imaging like SFDI, the image only for the ambient light is taken with the projection turned off. Motion artifact is another problem of SFDI, which arises when the specimen moves while switching multiple projection patterns or illumination wavelengths. To suppress motion artifacts, we are able to take advantage of the 8-tap CMOS image sensor's capabilities such as fast charge transfer and multiple exposure. We shorten the exposure time for each projection pattern, and repeat the exposure cycle multiple times. Although high-frame-rate cameras are useful to suppress the motion artifact, the hardware and computational costs will be higher due to the high data rate. In addition, shortened exposure time will degrade the signal to noise ratio. Our multi-tap image sensors are promising because motion artifacts and ambient light can be suppressed at the video rates.

In this paper, the principle of three-band SFDI with an 8-tap CMOS image sensor and the Hilbert transform is explained and experimentally verified.

2. SPATIAL FREQUENCY DOMAIN IMAGING USING MULTI-TAP CMOS IMAGE SENSOR

2.1. Multi-tap CMOS image sensor

Multi-tap CMOS image sensor pixels are composed of a single photodiode and multiple charge storage areas and charge transfer gates that control the charge transfer of the photogenerated charges in the photodiode to one of the charge storage areas. A pair of the charge storage area and transfer gate is referred as a tap. We have developed a lateral electric field modulator (LEFM) [4], which enables ultrafast charge transfer and is suitable for increasing the number of taps. Two to 8-tap pixels have been demonstrated[1, 5]. Fig. 2.1 shows the pixel structure, where PD, SD, G1-4, FD1-4 are photodiode, storage diodes, charge transfer gates, and floating diffusions that work as a voltage sensing node. The gates on both sides of the charge transfer path form an almost constant electric field along the charge transfer path to achieve high-speed charge transfer. By turning on the gates one by one, the photogenerated charges in PD are transferred to each tap and stored.

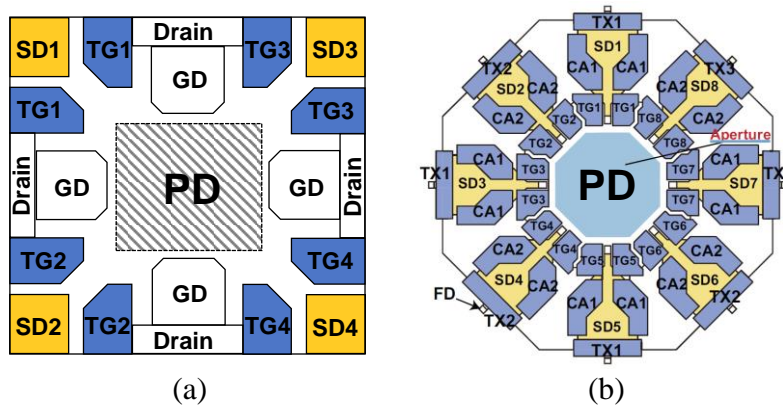


Fig. 2.1 : Examples of multi-tap pixel structures
(a) 4-tap sensor (SD works as FD) (b) 8-tap sensor

2.2. Estimation of absorption and reduced scattering coefficient by SFDI

In SFDI, the subject is illuminated typically with a DC or a sinusoidal (AC) pattern light. The AC patterns is written by Eq. 2.1, where S_0 , M_0 , f_x , and α are the light intensity, modulation, spatial frequency, and spatial phase of the pattern[6].

$$I_0 = \frac{S_0}{2} [1 + M_0 \cos(2\pi f_x + \alpha)] \quad (2.1)$$

The reflected intensity is shown in Eq. 2.2 using the DC reflectance, M_{DC} , and the AC reflectance, M_{AC} .

$$I = I_{DC} + I_{AC} = M_{DC}(x) + M_{AC}(x, f_x) \cdot \cos(2\pi f_x + \alpha) \quad (2.2)$$

In this paper, to measure the AC reflectance, the images for two spatial phases, $\alpha = 0, \frac{\pi}{2}$ [rad] are selected. When the pixel values of the DC and AC images are given by $I_0, I_{\frac{\pi}{2}}$, and I_{DC} , M_{DC} and M_{AC} at a position x are expressed by Eq. 2.3-4.

$$M_{DC}(x) = I_{DC} \quad (2.3)$$

$$M_{AC}(x, f_x) = \left\{ (I_0 - I_{DC})^2 + \left(I_{\frac{\pi}{2}} - I_{DC} \right)^2 \right\}^{\frac{1}{2}} \quad (2.4)$$

M_{DC} and M_{AC} are the amplitude reflectance. Note that the measured values include the effects of the intensity of the light source, f-number of lens, and so on. To convert the pixel values to the reflectance, it is necessary to calibrate the reflectance

of the specimen using a reference phantom with known optical properties. Using the measured $M_{DC}^{(ref)}$, $M_{AC}^{(ref)}$ for the reference phantom and the calculated reflectance, $M_{DC0}^{(ref)}$, $M_{AC0}^{(ref)}$, given by the Monte Carlo simulation, the reflectance of the specimen after calibration, $M_{DC}^{(cal)}$, $M_{AC}^{(cal)}$, are expressed as follows:

$$M_{DC}^{(cal)} = M_{DC} \times \frac{M_{DC0}^{(ref)}}{M_{DC}^{(ref)}} \quad (2.5)$$

$$M_{AC}^{(cal)} = M_{AC} \times \frac{M_{AC0}^{(ref)}}{M_{AC}^{(ref)}} \quad (2.6)$$

Using these calibrated values, the absorption and reduced scattering coefficients, μ_a and μ'_s are estimated from a look-up table (LUT), which are created by Monte Carlo simulation based on an appropriate tissue model.

2.3. Estimation of biochromophore concentrations and scattering parameters

Biochromophores such as water, oxy-/deoxy-hemoglobin, and melanin have different absorption spectra and they are will characterized[7]. In multi-band SFDI, μ_a is measured at multiple wavelengths and estimate biochromophore concentrations by fitting the measured μ_a 's with known absorption spectra of the biochromophores[8]. μ_a measured at a certain wavelength λ is represented by a weighted linear sum of the molar absorbance of the biochromophores, as shown in Eq. 2.7, where c_i and $\varepsilon_i(\lambda)$ are the concentration and molar absorbance of biochromophores.

$$\mu_a(\lambda) = \ln 10 \sum c_i \varepsilon_i(\lambda) \quad (2.7)$$

Total hemoglobin and tissue oxygen saturation, c_{tHB} and StO_2 , which are good indications of metabolism are defined by Eq. 2.8-9, where oxy-/deoxy-hemoglobin concentrations are denoted by c_{HB} and c_{HHb} .

$$c_{tHB} = c_{O_2Hb} + c_{HHb} \quad (2.8)$$

$$StO_2 = \frac{c_{O_2Hb}}{c_{O_2Hb} + c_{HHb}} \quad (2.9)$$

One of the advantages of SFDI is that SFDI provides the reduced scattering coefficients as well as the absorption coefficient. By fitting the measured reduced scattering coefficients at multiple wavelengths with the following equation, the scattering parameters, a and b , are obtained[9]. Note that a and b are dependent on the density and size of the scatterers, respectively. Since a and b change drastically depending on the burn severity, they are useful in diagnosis.

$$\mu'_s(\lambda) = a \left(\frac{\lambda}{500 \text{ nm}} \right)^{-b} \quad (2.10)$$

2.4. Suppression of ambient light and motion artifacts with multi-tap CMOS image sensors

In the SFDI based on a multi-tap CMOS image sensor, the sensor, projector, and LEDs are all synchronized. A specific combination of the projection pattern and illumination wavelength is assigned to each tap. An example of the charge transfer control signals for four-tap CMOS image sensors is shown in Fig. 2.2. In our previous study, three sinusoidal patterns with different phases were assigned to tap-1 to tap-3. Tap-4 is used to capture an ambient light image. The bias by the ambient light is removed by subtracting the signal from the signals of the other taps. Because multi-band SFDI requires multiple projection patterns and illumination wavelengths, motion artifacts are generated when the subject moves while chaging the projection. Motion artifacts can be suppressed by shortening the exposure time. However, the signal to noise ratio decreases. In our proposed method, we repeat the projection multiple times without reading images, so that signal levels are kept high due to the multiple exposure.

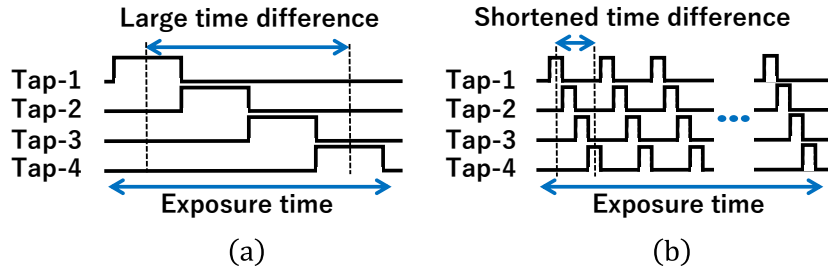


Fig. 2.2 : Charge transfer control signal
(a) Repeat one time (b) Multiple repetitions

3. THREE-WAVELENGTH SFDI USING HILBERT TRANSFORM

3.1. Hilbert transform

To obtain the metabolic information, it is necessary to estimate the concentrations of oxy-/deoxy-hemoglobin, that requires measurement at more than two wavelengths if melanin exists. The conventional SFDI requires three images for each wavelength. However, it is not easy to increase the number of taps more than eight due to the limitations of pixel area and fill factor. As demonstrated in Ref. [10], the Hilbert transform is useful to reduce the number of projection patterns in SFDI. In this study, we reduce the number of projection patterns to two by using the Hilbert transform and measure at three wavelengths with an 8-tap image sensor. The Hilbert transform is to obtain the components of a signal whose phase is shifted by $\frac{\pi}{2}$ rad. Along the wave vector of the projected pattern, the following imaginary function, where f_x is spatial frequency is multiplied to the Fourier spectrum of a captured image after subtracting the DC image.

$$S = \begin{cases} -j (f_x > 0) \\ j (f_x < 0) \\ 0 (f_x = 0) \end{cases} \quad (3.1)$$

3.2. Three-wavelength SFDI using 8-tap CMOS image sensor and Hilbert transform

Table 3.1 shows the assignment of projection patterns and wavelength to eight taps of the image sensor to perform three-band SFDI.

Table 3.1 : Projection patterns in three-wavelength SFDI

λ of LED	λ_1 (660 nm)		λ_2 (780 nm)		λ_3 (850 nm)		Ambi-ent	Drain
	DC	sin	DC	sin	DC	sin		
Captured images								
Tap #	1	2	3	4	5	6	7	8

From the images taken for sinusoidal patterns for three wavelengths, images for the cosine patterns are created by the Hilbert transform. Tap-7 captures the ambient light image for removing the ambient light. Tap-8 is used for draining photogenerated charges during the image readout. M_{DC} and M_{AC} are measured at every wavelength, μ_a and μ'_s are estimated by referring to the LUT based on a bulk tissue model. Then, biochromophore concentrations and scattering parameters are estimated as mentioned above.

4. EXPERIMENTAL RESULTS

4.1. Experimental conditions

c_{tHB} , StO_2 , a , and b of a human wrist were measured using the proposed three-band SFDI. Table 4.1 shows the experimental condition. The fitting was performed only with oxy-/deoxy-hemoglobin because the estimation including melanin did not work well with a bulk tissue model.

Table 4.1 : Experimental condition of three-band SFDI

Specimen	Human forearm
Environment	Dark room
Spatial frequency	0.10 mm^{-1}
Averaged number	100
Repeated number	1

Table 4.2 shows the specifications of the sensor used this study.

Table 4.2 : Specifications of 8-tap CMOS image sensor

Pixel size	$22.4 \times 22.4 \text{ } [\mu\text{m}^2]$
Pixel number	$134(\text{H}) \times 150(\text{V})$
Frame rate	6.28 [fps]
Exposure time	About 70 [ms]
Tap number	8

Fig 4.1 shows the optical system used this study.

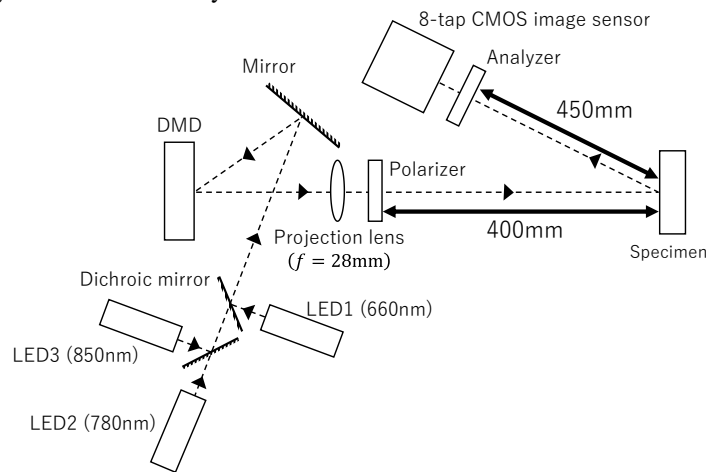


Fig. 4.1 : The optical system

4.2. Experimental results

Fig. 4.1 shows the experimental results. The average value of StO_2 was 65.8%, which was slightly different from the literature value of 74% [11]. This error could be caused by the influence of melanin. In the future work, two-layer models should be considered. The most crucial problem was the signal to noise ratio of the 8-tap CMOS image sensor. Because the dark current of the sensor used in this experiment, averaging 100 frames was necessary. Probably due to the high noise level of the sensor, scattering parameter, b , became very noisy even with averaging. Improvement of the sensor performance especially of dark current and photosensitivity is necessary.

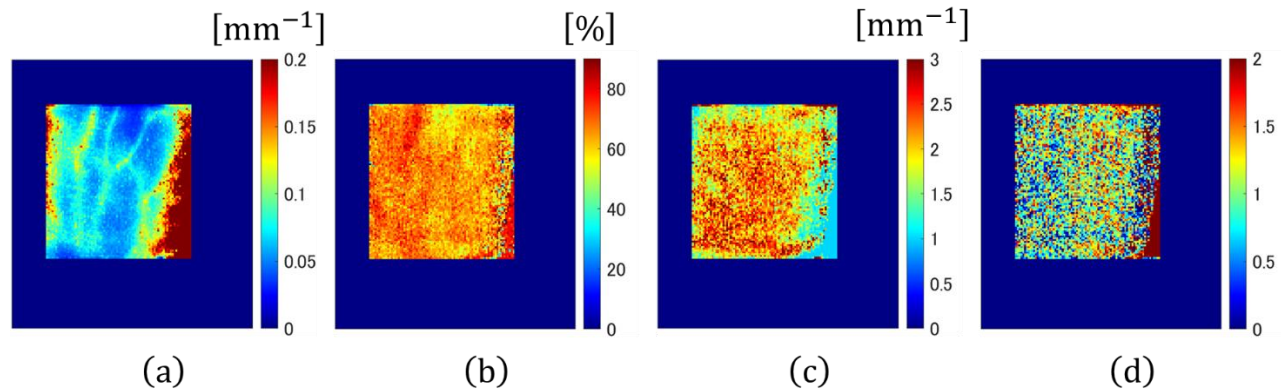


Fig. 4.1 : Results of three-band SFDI

5. CONCLUSION

We proposed the three-band SFDI method using an 8-tap CMOS image sensor and the Hilbert transform. We successfully measured the total hemoglobin, tissue oxygen saturation, and scattering parameters using the proposed method. In the future, we would like to investigate the fitting of a multilayer model considering melanin.

6. ACKNOWLEDGEMENTS

This work was supported in part by JSPS KAKENHI Grant Number 18H05240 and 21H04557.

REFERENCES

- [1] Y. Shirakawa, K. Yasutomi, K. Kagawa, S. Aoyama, and S. Kawahito, "An 8-tap CMOS lock-in pixel image sensor for short-pulse time-of-flight measurements," *MDPI Sensors*, Vol. 20, Issue 4, Article 1040 (2020).
- [2] K. P. Nadeau, A. J. Durkin, and B. J. Tromberg, "Advanced demodulation technique for the extraction of tissue optical properties and structural orientation contrast in the spatial frequency domain," *Journal of Biomedical Optics*, Vol. 19, No. 5, 056013 (2014).
- [3] K. G. Larkin, D. J. Bone, and M. A. Oldfield, "Natural demodulation of two-dimensional fringe patterns. I. General background of the spiral phase quadrature transform," *Journal of the Optical Society of America A*, Vol. 18, No. 8 (2001).
- [4] S. Kawahito, G. Baek, Z. Li, S. Han, M. Seo, K. Yasutomi and K. Kagawa, "CMOS lock-in pixel image sensors with lateral electric field control for time-resolved imaging," *International Image Sensor Workshop*, 10.06, pp. 1417-1429 (2013).
- [5] K. Kondo, K. Yasutomi, K. Yamada, A. Komazawa, Y. Handa, Y. Okura, T. Michiba, S. Aoyama, and S. Kawahito, *Solid State Devices and Materials*, pp. 601-602 (2018).
- [6] D. J. Cuccia, F. Bevilacqua, A. J. Durkin, F. R. Ayers, and B. J. Tromberg, "Quantitation and mapping of tissue optical properties using modulated imaging," *Journal of Biomedical Optics*, vol. 14, no. 2, (2009).
- [7] J. Weber, P. C. Beard, and S. E. Bohndiek, "Contrast agents for molecular photoacoustic imaging," *Nature Methods*, Vol. 13, 639-650 (2016).
- [8] A. Mazhar, S. Dell, D. J. Cuccia, S. Gioux, A. J. Durkin, J. V. Frangioni, and B. J. Tromberg, "Wavelength optimization for rapid chromophore mapping using spatial frequency domain imaging," *Journal of Biomedical Optics*, Vol. 24, No. 4, pp. 639-651(2009).
- [9] David J. Cuccia, David Abookasis, Ron D. Frostig, and Bruce J. Tromberg. "In Vivo Optical Imaging of Brain Function, 2nd edition," *Frontiers in Neuroscience*, (2019)
- [10] K. P. Nadeau, A. J. Durkin, and B. J. Tromberg, "Advanced demodulation technique for the extraction of tissue optical properties and structural orientation contrast in the spatial frequency domain," *Journal of Biomedical Optics*, Vol. 19, No. 5, 056013 (2014).

- [11] R. M. P. Doornbos, R. Lang, M. C. Aalders, F. W. Cross, and H. J. C. M. Sterenborg, "The determination of in vivo human tissue optical properties and absolute chromophore concentrations using spatially resolved steady-state diffuse reflectance spectroscopy," *Physics in Medicine and Biology*, Vol. 44, No. 4, 967 (1999).